
Glitter in the Darkness? Nonfibrillar β -Amyloid Plaque Components Significantly Impact the β -Amyloid PET Signal in Mouse Models of Alzheimer Disease

Gloria Biechele*¹, Laura Sebastian Monasor*^{2,3}, Karin Wind¹, Tanja Blume^{1,2}, Samira Parhizkar⁴, Thomas Arzberger², Christian Sacher¹, Leonie Beyer¹, Florian Eckenweber¹, Franz-Josef Gildehaus¹, Barbara von Ungern-Sternberg¹, Michael Willem⁵, Peter Bartenstein^{1,6}, Paul Cumming^{7,8}, Axel Rominger^{1,7}, Jochen Herms^{2,6,9}, Stefan F. Lichtenthaler^{2,6,10}, Christian Haass^{2,5,6}, Sabina Tahirovic*², and Matthias Brendel*^{1,6}

¹Department of Nuclear Medicine, University Hospital of Munich, LMU Munich, Munich, Germany; ²German Center for Neurodegenerative Diseases Munich, Munich, Germany; ³Graduate School of Systemic Neuroscience, Ludwig-Maximilians-University Munich, Munich, Germany; ⁴Department of Neurology, Washington University, St. Louis, Missouri; ⁵Chair of Metabolic Biochemistry, Biomedical Center, Faculty of Medicine, LMU Munich, Munich, Germany; ⁶Munich Cluster for Systems Neurology, Munich, Germany; ⁷Department of Nuclear Medicine, Inselspital, University Hospital Bern, Bern, Switzerland; ⁸School of Psychology and Counselling and IHBI, Queensland University of Technology, Brisbane, Australia; ⁹Center of Neuropathology and Prion Research, University of Munich, Munich, Germany; and ¹⁰Neuroproteomics, School of Medicine, Klinikum Rechts der Isar, Technical University of Munich, Munich, Germany

β -amyloid (A β) PET is an important tool for quantification of amyloidosis in the brain of suspected Alzheimer disease (AD) patients and transgenic AD mouse models. Despite the excellent correlation of A β PET with gold standard immunohistochemical assessments, the relative contributions of fibrillar and nonfibrillar A β components to the in vivo A β PET signal remain unclear. Thus, we obtained 2 murine cerebral amyloidosis models that present with distinct A β plaque compositions and performed regression analysis between immunohistochemistry and A β PET to determine the biochemical contributions to A β PET signal in vivo. **Methods:** We investigated groups of *App*^{NL-G-F} and APPPS1 mice at 3, 6, and 12 mo of age by longitudinal ¹⁸F-florbetaben A β PET and with immunohistochemical analysis of the fibrillar and total A β burdens. We then applied group-level intermodality regression models using age- and genotype-matched sets of fibrillar and nonfibrillar A β data (predictors) and A β PET results (outcome) for both A β mouse models. An independent group of double-hit APPPS1 mice with dysfunctional microglia due to knockout of triggering receptor expression on myeloid cells 2 (*Trem2*^{-/-}) served for validation and evaluation of translational impact. **Results:** Neither fibrillar nor nonfibrillar A β content alone sufficed to explain the A β PET findings in either AD model. However, a regression model compiling fibrillar and nonfibrillar A β together with the estimate of individual heterogeneity and age at scanning could explain a 93% of variance of the A β PET signal ($P < 0.001$). Fibrillar A β burden had a 16-fold higher contribution to the A β PET signal than nonfibrillar A β . However, given the relatively greater abundance of nonfibrillar A β , we estimate that nonfibrillar A β produced 79% \pm 25% of the net in vivo A β PET signal in *App*^{NL-G-F} mice and 25% \pm 12% in APPPS1 mice. Corresponding

results in separate groups of APPPS1/*Trem2*^{-/-} and APPPS1/*Trem2*^{+/+} mice validated the calculated regression factors and revealed that the altered fibrillarity due to *Trem2* knockout impacts the A β PET signal. **Conclusion:** Taken together, the in vivo A β PET signal derives from the composite of fibrillar and nonfibrillar A β plaque components. Although fibrillar A β has inherently higher PET tracer binding, the greater abundance of nonfibrillar A β plaque in AD-model mice contributes importantly to the PET signal.

Key Words: amyloid; fibrillar; nonfibrillar; PET signal; mouse

J Nucl Med 2022; 63:117–124
DOI: 10.2967/jnumed.120.261858

PET for β -amyloid (A β) is now widely used for identification and quantification of amyloidosis in the brain of suspected Alzheimer disease (AD) patients (1) and has been incorporated into the current research framework for diagnostic recommendations in AD (2). Here, the A β status (A) identified by PET serves for diagnosis, together with biomarkers for tau and neuronal injury (2). Furthermore, A β PET is used as an inclusion criterion in anti-amyloid immunotherapy clinical trials (3) and as a progression biomarker for therapy evaluation in these trials (4). In the preclinical setting, A β PET has also become a useful tool for the dynamic assessment of neuropathology in transgenic A β mouse models (5,6). Despite the excellent correlation of A β PET with immunohistochemical gold standard assessments of amyloidosis in patients (7,8) and mouse models of AD (6,9), there has remained an uncertainty about the relative contributions of fibrillar and nonfibrillar A β components in plaques to the A β PET signal in vivo. This research gap needs to be closed because the 2 forms have differing neurotoxicity, and there is evidence that alterations in AD-related genes such as *TREM2* (triggering receptor expressed on myeloid cells 2) and *APOE* (apolipoprotein E) alter the net A β plaque fibrillarity, which would consecutively bias the relationship between plaque density and A β PET binding in vivo (5).

Received Dec. 18, 2020; revision accepted Apr. 13, 2021.

For correspondence or reprints, contact Matthias Brendel (matthias.brendel@med.uni-muenchen.de).

*Contributed equally to this work.

Published online May 20, 2021.

Immediate Open Access: Creative Commons Attribution 4.0 International License (CC BY) allows users to share and adapt with attribution, excluding materials credited to previous publications. License: <https://creativecommons.org/licenses/by/4.0/>. Details: <http://jnm.snmjournals.org/site/misc/permission.xhtml>.

COPYRIGHT © 2022 by the Society of Nuclear Medicine and Molecular Imaging.

A human autopsy-validated ^{18}F -florbetaben PET study showed preliminary evidence that diffuse plaques may make only a minor contribution to the net A β PET signal (10). However, autopsy-controlled data with ^{18}F -flutemetamol in vivo (11) and comprehensive in vitro data (12) indicated that the binding of that structurally distinct tracer to diffuse plaques also contributes to the net PET signal. Furthermore, our recent preclinical study revealed a discernible A β PET signal in *App^{NL-G-F}* mice (13), although this model displays only very limited fibrillar A β pathology (14). Therefore, we aimed to quantify the contributions of fibrillar and nonfibrillar plaque components to the A β PET signal in vivo in AD-model mice.

We recently demonstrated that the *App^{NL-G-F}* and APPPS1 mouse models exhibit differences in A β plaque fibrillarity (14), such that a comparative study of these mice could help to determine the effect of fibrillarity on A β PET signal in vivo. Thus, we combined a standardized preclinical ^{18}F -florbetaben PET study with immunohistochemical characterization of fibrillar versus nonfibrillar A β in *App^{NL-G-F}* and APPPS1 mice examined at different pathologic stages. We then developed a regression model for immunohistochemistry and A β PET to establish the relative proportions of fibrillar and nonfibrillar sources in the A β PET signal in vivo. Furthermore, we validated the calculated regression factors in an independent cohort of APPPS1/Trem2^{-/-} and APPPS1/Trem2^{+/+} mice and tested a hypothesis that the nonfibrillar A β pool contributes more to the A β PET signal in APPPS1/Trem2^{-/-} mice than in APPPS1/Trem2^{+/+} mice.

MATERIALS AND METHODS

Experimental Design

All experiments were performed in compliance with the National Guidelines for Animal Protection, Germany, and with the approval of the regional animal committee (Regierung Oberbayern) and were overseen by a veterinarian. Animals were housed in a temperature- and humidity-controlled environment with a 12-h light-dark cycle and with free access to food (Sniff) and water. We conducted longitudinal ^{18}F -florbetaben A β PET imaging in cohorts of female *App^{NL-G-F}* ($n = 18$) and APPPS1 ($n = 14$) mice at 3, 6, and 12 mo of age, together with an age- and sex-matched group of wild-type ($n = 8$) mice. Of the A β mouse models, 56% had their baseline examination at 3 mo of age and the remaining 44% were imaged from 6 to 12 mo of age. All mice of each model originated from the same breeding colony. To exclude batch effects within each modality, we used separate cohorts of mice (14) for immunohistochemistry analyses of fibrillar and nonfibrillar A β plaque components in wild-type and AD-model mice ($n = 3$ –4) at 3, 6, and 12 mo of age. We then applied intermodality regression models to separate the relative contributions of fibrillar and nonfibrillar A β plaque components to A β PET signals in the 2 strains.

Animal Models

APPS1 (APPS1-21) mice show extensive fibrillar A β plaque pathology, first evident at 6–8 wk of age (15). In contrast, *App^{NL-G-F}* (*App^{NL-G-F/NL-G-F}*) is a murine model with relatively limited fibrillar A β plaque pathology but showing A β PET signal from 8 wk of age in homozygous mice (16,17). Wild-type controls were C57BL/6 mice.

PET Imaging

PET Data Acquisition, Reconstruction, and Postprocessing. For all PET procedures, radiochemistry, data acquisition, and image preprocessing were conducted according to an established, standardized protocol (6). In brief, we obtained ^{18}F -florbetaben A β PET

recordings (average dose, 12.1 ± 1.8 MBq) with an emission window of 30–60 min after injection.

PET Image Analysis. We performed all analyses using PMOD (version 3.5; PMOD Technologies). Normalization of attenuation-corrected emission images to SUV ratio images was performed using previously validated periaqueductal gray matter (18) and white matter reference regions for the *App^{NL-G-F}* and APPPS1 mouse models, respectively (5). We analyzed the wild-type mice separately with both reference regions to serve as controls for the A β mouse models. Bilateral neocortical volumes of interest (15 mm^3) matching the region of interest in the immunohistochemistry analysis were applied for calculation of forebrain-to-white matter SUV ratio or forebrain-to-periaqueductal gray matter SUV ratio.

Immunohistochemical Analysis

Groups of APPPS1 and *App^{NL-G-F}* mice at an age of 3 mo ($n = 4$), 6 mo ($n = 3$), and 12 mo ($n = 4$) were transcardially perfused with ice-cold phosphate-buffered saline (0.1 M) followed by 4% paraformaldehyde, after being cryopreserved in 30% sucrose. The mouse tissue used for immunohistochemical analysis included some of the APPPS1 and *App^{NL-G-F}* mouse brains used in our previous publication (14). All stainings and analyses were performed newly for the purpose of the present study. We collected 30- μm -thick coronal sections for free-floating immunostaining. We used the 3552 antibody (1:5,000 (19)) to label total A β , and we used thiazine red (2 μM ; Sigma) to stain the fibrillar A β . Twenty-four images were acquired in 4 coronal sections (6 images per section) in regions matching PET using a confocal microscope ($\times 20$ dry objective, TCS SP5; Leica). Given the prominent differences in the levels of fibrillar A β between the APPPS1 and *App^{NL-G-F}* mice, the confocal settings were optimized for each mouse model to acquire the thiazine red signal. For the 3- and 6-mo-old *App^{NL-G-F}* mice, the averaging and accumulation confocal functions were set to 2, to better detect the thiazine red signal. An in-house-programmed macro from ImageJ (NIH) was used to analyze the total and fibrillar A β coverage.

As a validation analysis, we reanalyzed data from a previous study that included immunohistochemistry markers for fibrillar (x-34) and total (3552) A β components of A β plaques (5). Immunohistochemistry was obtained from APPPS1/Trem2^{+/+} and APPPS1/Trem2^{-/-} mice (3 and 6 mo, $n = 4$; 12 mo, $n = 8$). A β PET data were analyzed by the processing pipeline described above and at the same time points for both genotypes (APPS1/Trem2^{+/+}: three 3-mo-old, ten 6-mo-old, and ten 12-mo-old mice; APPPS1/Trem2^{-/-}: seven 3-mo-old, nine 6-mo-old, and seven 12-mo-old mice). Furthermore, for validation purpose we obtained A β coverage for fibrillar (methoxy-x04 or x-34) and total (3552) A β components at 13 mo of age in the PET cohorts. In all datasets, nonfibrillar A β was calculated by subtraction of fibrillar A β from total A β (percentage nonfibrillar area = percentage total area – percentage fibrillar area).

Statistics

Prism (version 8.43; GraphPad Software, LCC) was used for all statistical tests. A P value of less than 0.05 was considered to be significant for rejection of the null hypothesis.

Group-Level Analysis. Nonfibrillar A β , fibrillar A β , and the A β PET z score were compared between *App^{NL-G-F}* and APPPS1 mice at different ages by an unpaired Student t test. Mean values of each of the 3 readouts from the *App^{NL-G-F}* and APPPS1 groups at different ages were subject to a linear regression analysis. The area between the regression plots served as an index of the potential bias in the estimates of A β pathology by A β PET.

Individual-Level Analysis. We applied regression models using the A β PET z score of all investigated mice in both models as an outcome variable. Fibrillar A β and nonfibrillar A β estimates deriving

from all age- and genotype-matched mouse groups were used as predictors, and heterogeneity of individual mice with respect to PET results and age were used as additional covariates. We defined heterogeneity as the deviation of individual mice in each genotype from their group mean at each time point. The regression coefficients for fibrillar A β and nonfibrillar A β were extracted to calculate their relative contributions to the A β PET signal. Bootstrapping was performed with 1,000 random samples.

Validation Analysis. The derived regression coefficients were applied to immunohistochemistry analysis of independent samples of APPPS1/Trem2^{+/+} and APPPS1/Trem2^{-/-} mice. The predicted A β PET z scores were compared with the actual A β PET z scores in vivo, and the deviation between the predicted and actual A β PET z scores was compared with separate consideration of both plaque components and sole consideration of fibrillar A β . The bias resulting from consideration of only fibrillar A β was calculated as a function of longitudinal changes in the A β PET signal in the comparison of APPPS1/Trem2^{+/+} and APPPS1/Trem2^{-/-} mice.

RESULTS

Separate Quantification of Fibrillar or Nonfibrillar A β Plaque Deposition Fails to Explain the A β PET Signal

First, we performed a direct standardized comparison of nonfibrillar and fibrillar A β estimates by immunohistochemistry and A β PET between *App*^{NL-G-F} and APPPS1 mouse models at different ages. Nonfibrillar A β area coverage of *App*^{NL-G-F} mice exceeded that of APPPS1 mice at 3 and 6 mo of age, whereas APPPS1 mice had higher nonfibrillar A β area coverage at 12 mo of age (Figs. 1A and 2). Fibrillar A β area coverage was significantly higher in APPPS1 mice than in *App*^{NL-G-F} mice at all ages studied (Figs. 1B and 2). Immunohistochemically assessed area coverage values did not differ between the immunohistochemistry cohorts and the PET cohorts at 12/13 mo of age (all $P > 0.05$, Supplemental Fig. 1; supplemental materials are available at

<http://jnm.snmjournals.org>). A β PET z scores of *App*^{NL-G-F} and APPPS1 mice are provided and illustrated in Figures 1C and 1D. There were no interindividual SUV ratio differences between mice imaged 3 times, at 3, 6, and 12 mo, and mice imaged only twice, at 6 and 12 mo (all $P > 0.05$, Supplemental Fig. 2). A β PET showed significantly higher standardized differences in APPPS1 mice than in *App*^{NL-G-F} mice at 6 and 12 mo, whereas there were no significant differences at 3 mo of age (Fig. 1C). Plotting of A β PET results as a linear function of nonfibrillar or fibrillar A β at different ages indicated a mismatch between the 2 mouse models (Fig. 1E). Plotting of fibrillar A β as a linear function of nonfibrillar A β coverage underpinned that APPPS1 mice had a higher proportion of fibrillar A β than did *App*^{NL-G-F} mice (Fig. 1E). The comparison of the linear functions of both mouse models (the area transected by the regression lines) indicated that A β PET underestimated the proportion of nonfibrillar A β in *App*^{NL-G-F} mice (-2.08 z score units) but overestimated the proportion of fibrillar A β in *App*^{NL-G-F} mice ($+2.36$ z score units). Thus, neither fibrillar nor nonfibrillar A β alone could explain the combined A β PET findings.

Nonfibrillar A β Contributes Significantly to the A β PET Signal

Next, we hypothesized that a combined model of nonfibrillar and fibrillar A β components could improve the explanation of variance in the A β PET signals. To test this hypothesis, we established a multiple-regression model using all available combinations of age- and genotype-matched A β PET-immunochemistry or histochemistry estimates with inclusion of all *App*^{NL-G-F} and APPPS1 mice.

Simplified regression models with either fibrillar or nonfibrillar A β as predictors of the A β PET z score explained 50% and 32% of the variance in A β PET, respectively (both $P < 0.001$, Table 1). Combined consideration of fibrillar A β and nonfibrillar A β as predictors of the A β PET z score increased the explained variance to 57% ($P < 0.001$, Table 1; Fig. 3A), and fibrillar ($\beta = 0.563$, $P =$

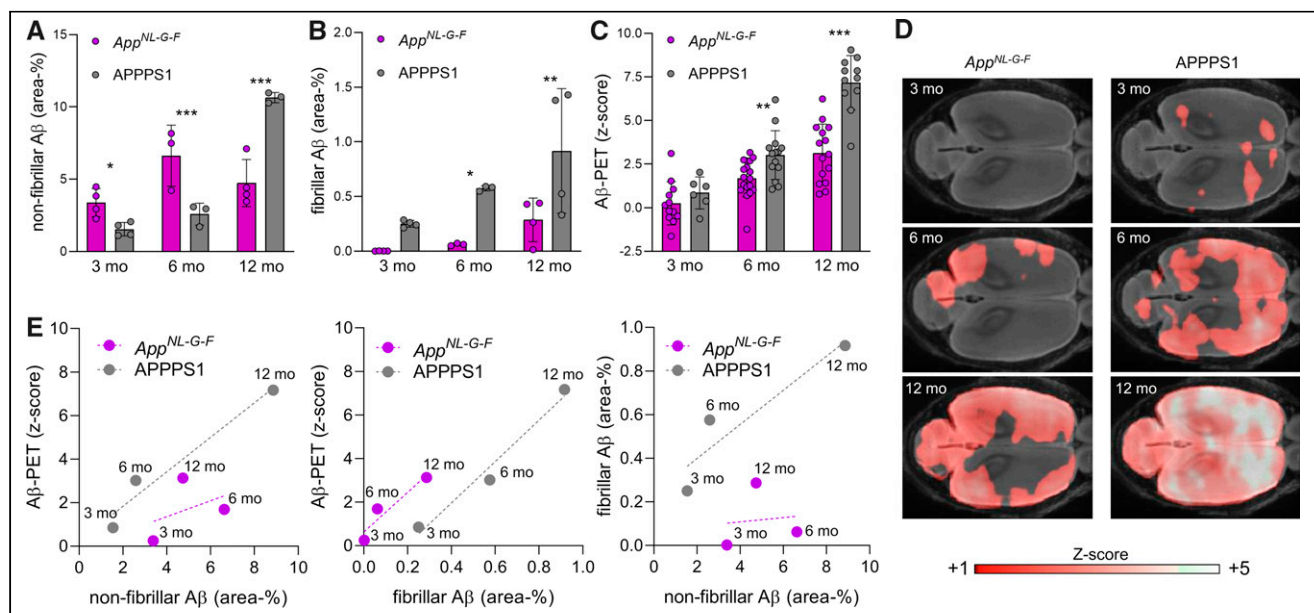


FIGURE 1. (A–D) Quantitation of nonfibrillar A β (A), fibrillar A β (B), and A β PET signal z scores (C) in neocortex of *App*^{NL-G-F} and APPPS1 mice at 3, 6, and 12 mo of age, together with axial images of groupwise PET z scores projected on MRI standard template (D). (E) Correlation plots of associations between immunohistochemistry or histochemistry markers and PET at different ages (group level) in comparison of both mouse models. * $P < 0.05$. ** $P < 0.01$. *** $P < 0.001$.

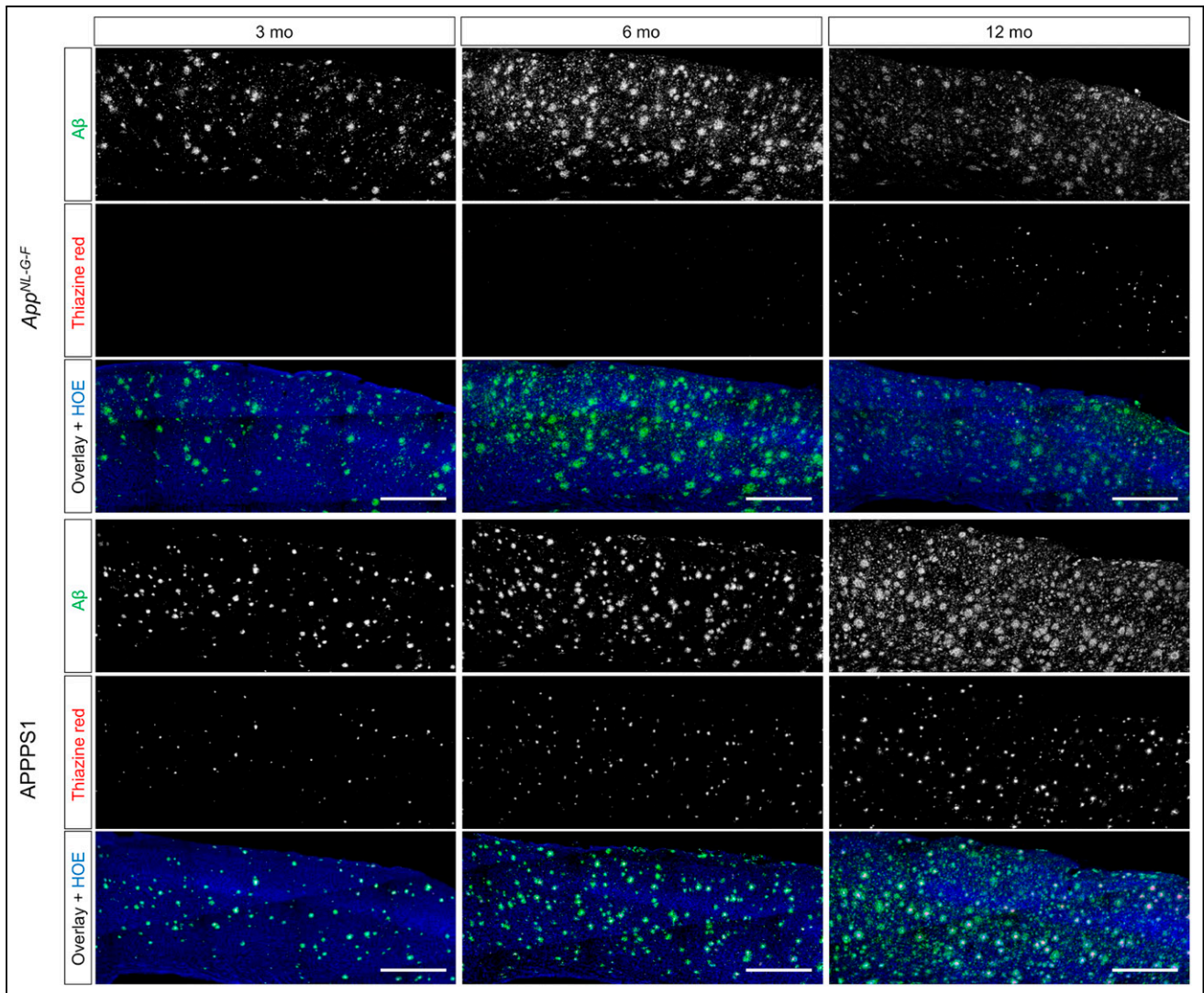


FIGURE 2. Representative images of immunocytochemistry and histochemistry. Total A β was assessed by 3552 staining, and fibrillar A β was assessed by thiazine red. Hoechst (HOE, blue) was used for nuclear visualization (scale bars, 500 μ m).

$1.11e^{-27}$) and nonfibrillar ($\beta = 0.309$, $P = 9.38e^{-11}$) A β were both strong and independent predictors of the A β PET z score.

A model including fibrillar and nonfibrillar A β components with the estimate of individual heterogeneity yielded 85% explanation of

variance of the A β PET signal (Fig. 3B), and further inclusion of age further increased the explanation of variance of the A β PET signal (93%, Fig. 3C). Thus, age-related factors influence, importantly, immunocytochemistry/histochemistry and PET signals (i.e., age-

TABLE 1

Coefficients of Determination and Regression Coefficients for Prediction of A β PET Signal by Fibrillar and Nonfibrillar A β Components, with Additional Factoring for Heterogeneity (in Mice with Equal Genotype at Single Time Point) and Age

Model	R^2	Corrected R^2	B Fibrillar	B Nonfibrillar	P
Fibrillar	0.499	0.497	4.414 (3.915–4.926)		<0.001
Nonfibrillar	0.324	0.322		0.477 (0.378–0.569)	<0.001
Fibrillar \times nonfibrillar	0.574	0.571	3.521 (2.954–4.041)	0.259 (0.178–0.341)	<0.001
Fibrillar \times nonfibrillar \times heterogeneity	0.854	0.852	3.521 (2.954–4.041)	0.259 (0.178–0.341)	<0.001
Fibrillar \times nonfibrillar \times heterogeneity \times age	0.928	0.927	2.810 (2.620–3.032)	0.146 (0.103–0.193)	<0.001

R^2 = coefficient of determination; B = regression coefficient.

Numbers in parentheses represent 95% CIs as assessed by bootstrapping with 1,000 random samples.

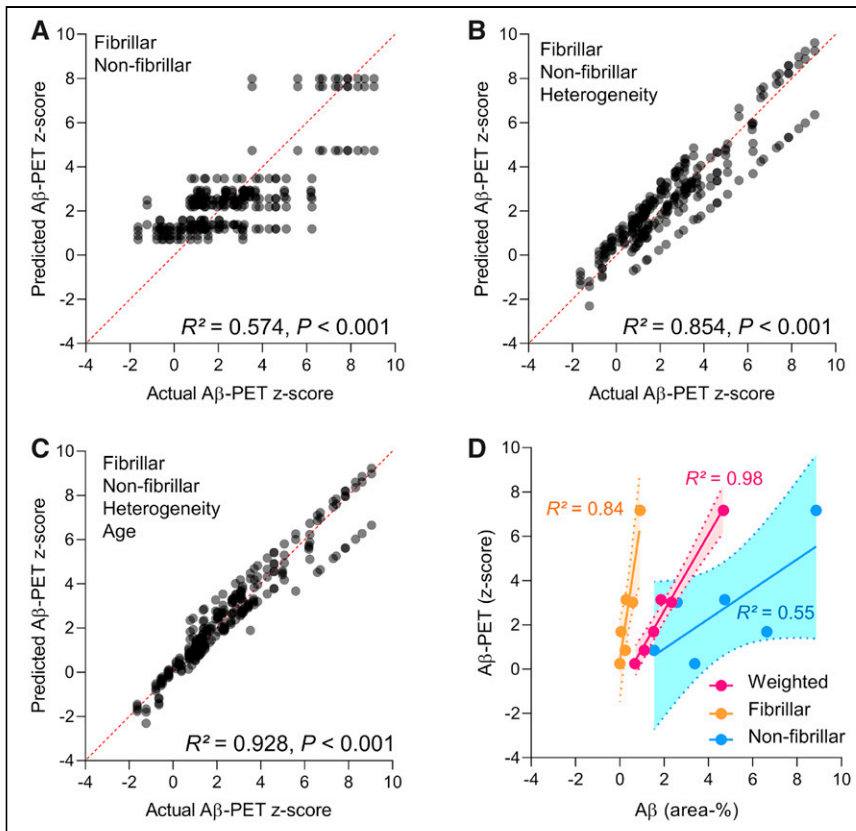


FIGURE 3. (A–C) Regression plots illustrate correlation between actual and predicted Aβ PET z score when using fibrillar Aβ and nonfibrillar Aβ as predictors and using individual heterogeneity and age as covariates. Regressions were calculated with total of 261 permutations between immunochemistry or histochemistry and PET endpoints using all available combinations with matched age and genotype. (D) Application of average regression factors for fibrillar ($B = 3.17$) and nonfibrillar ($B = 0.20$) Aβ on combined immunochemistry and histochemistry data for both models (group means per age).

dependent perfusion or partial-volume effects). We considered “fibrillar \times nonfibrillar \times heterogeneity” and “fibrillar \times nonfibrillar \times heterogeneity \times age” to be the most accurate models, and we calculated the mean regression coefficients from these 2 models to obtain the contributions of fibrillar Aβ and nonfibrillar Aβ to the PET signal. One percent area covered by fibrillar Aβ explained 3.17 PET z score units, and 1% area covered by nonfibrillar Aβ explained 0.20 PET z score units, thus indicating a 16-fold higher contribution of fibrillar than of nonfibrillar Aβ. The opposite edges of the 95% CIs, as assessed by bootstrapping, indicated a possible range between 11-fold and 26-fold for the relationship between fibrillary and nonfibrillar contributions to the Aβ PET signal. Application of this multiplicative factor to the direct comparison of group-averaged immunochemistry/histochemistry and Aβ PET scores in *App^{NL-G-F}* and APPPS1 mice at different ages confirmed the suitability of this model, as indicated by 98% explanation of the variance using weighted factors, compared with only 84% for isolated fibrillar and 55% for nonfibrillar plaque components (Fig. 3D).

Fibrillar and Nonfibrillar Plaque Components Have an Impact on Mice with Dysfunctional Microglia

Finally, we validated our results in independent cohorts of APPPS1 mice and made an additional investigation of the impact of Trem2 deficiency on the Aβ PET signal in these mice, given that Trem2 is a known driver of changes in the plaque fibrillarity.

Application of the regression factors to immunochemistry/histochemistry data indicated an excellent prediction of the actual Aβ PET signal in independent cohorts of APPPS1/Trem2^{-/-} and APPPS1/Trem2^{+/+} mice (Fig. 4A). APPPS1 mice with Trem2 loss of function showed a higher contribution of nonfibrillar plaque components to the Aβ PET signal (30% at 3 mo, 26% at 6 mo, and 24% at 12 mo) than did APPPS1 mice with intact Trem2 (4% at 3 mo, 15% at 6 mo, and 21% at 12 mo; Fig. 4A). A combined consideration of fibrillar Aβ and nonfibrillar Aβ predicted the actual PET signal more precisely than did sole consideration of fibrillar Aβ (Fig. 4B). Previously calculated increases in Aβ PET signal with age in these mice indicated a considerable bias when considering only the fibrillar Aβ component (Supplemental Fig. 3). In summary, microglial dysfunction altered the relative proportions of fibrillar and nonfibrillar Aβ, thus directly influencing the Aβ PET signal as a function of mouse age.

DISCUSSION

We provide the first—to our knowledge—in vivo analysis to elucidate the contributions of fibrillar and nonfibrillar plaque components to the Aβ PET signal. Our data clearly show that nonfibrillar plaque fractions have a significant impact on the net ¹⁸F-florbetaben binding to Aβ plaques of Aβ mouse models in vivo.

Although the resulting Aβ PET tracer signal is inherently 16-fold higher when comparing equal amounts of fibrillar and nonfibrillar Aβ, the larger proportions of nonfibrillar plaque components counterbalance the net contribution. We validated our regression model in an independent cohort of APPPS1 mice and extended the potential translational impact of our findings by showing that microglial dysfunction can influence the longitudinal Aβ PET signal via changing the relative proportions of fibrillar-to-nonfibrillar plaque components.

In various analyses of single amyloidosis mouse models, there was a strong agreement between Aβ PET and different immunochemistry or histochemistry markers for Aβ (9,20). It is widely acknowledged that the Aβ PET signal with ¹⁸F-florbetaben derives primarily from aggregated fibrillar Aβ, since this and other clinically approved Aβ PET tracers were derived from the chemical scaffold of thioflavin-T, which colors only fibrillar Aβ (21). However, a recent small-animal Aβ PET investigation from our lab (18) indicated that there could be discrepancies between immunochemistry/histochemistry and in vivo Aβ PET signals, if one attributes the entire PET signal to fibrillar Aβ. In fact, *App^{NL-G-F}* mice exhibited an only moderate Aβ PET signal, although their plaques were composed mainly of nonfibrillar Aβ (14). Therefore, we applied in this study a standardized ¹⁸F-florbetaben PET examination comparing *App^{NL-G-F}* and APPPS1 mice in conjunction with combined histochemical and immunohistochemical

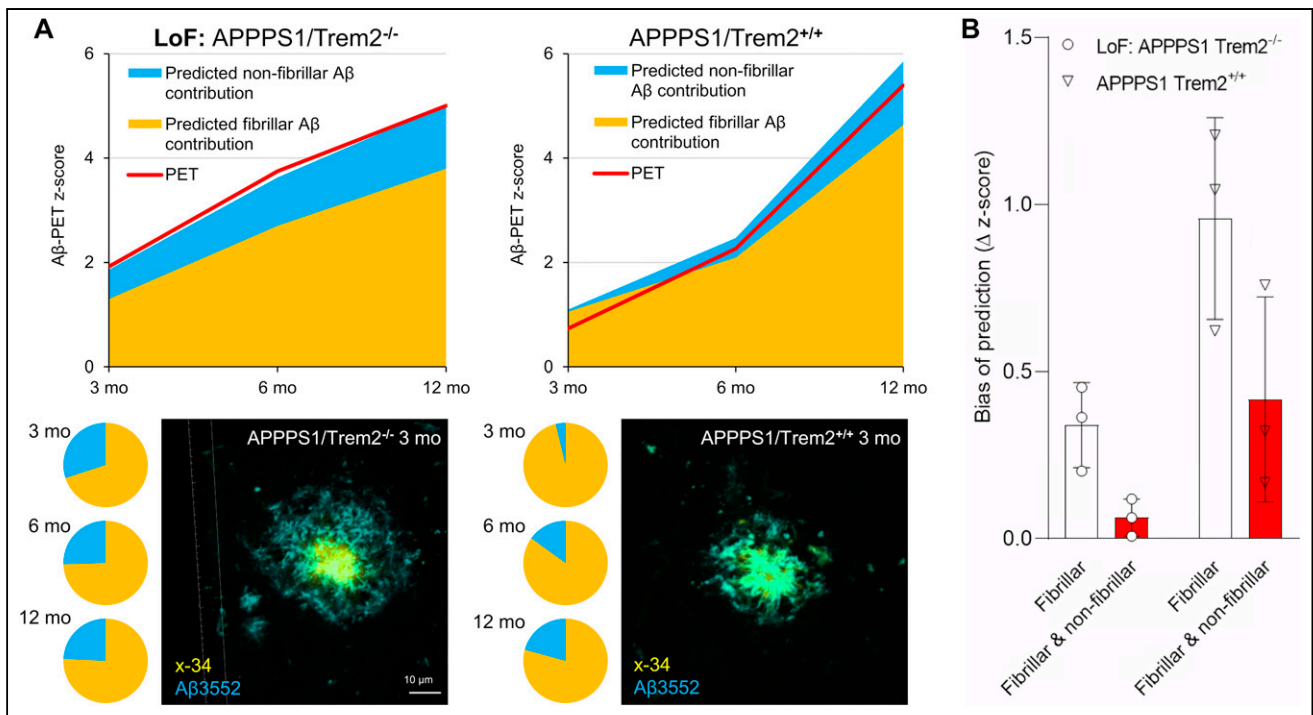


FIGURE 4. (A) z scores of measured A β PET signal and predicted fibrillar and nonfibrillar (blue) source components in independent cohort of APPPS1 mice with dysfunctional (Trem2^{-/-}) and intact (Trem2^{+/+}) microglia. Pie charts show fibrillar and nonfibrillar contributions to measured A β PET signals predicted by immunochemistry and histochemistry. Representative double staining of APPPS1/Trem2^{-/-} mouse shows more nonfibrillar A β (3552-positive) surrounding core (x-34-positive) than in APPPS1/Trem2^{+/+} mouse, both at 3 mo of age. (B) Bias of predicted z scores when only fibrillar or combination of fibrillar and nonfibrillar plaque contributions was considered. Analysis displays deviation of immuno/histochemically predicted A β PET values and actual A β PET signal. Each dot represents one age-related group of APPPS1/Trem2^{-/-} or APPPS1/Trem2^{+/+} mice (3 mo, 6 mo, 12 mo).

examination to elucidate the separate contributions of fibrillar and nonfibrillar A β sources to the in vivo A β PET signal. We performed PET acquisitions in both A β models and wild-type mice with identical housing conditions and using the same tomograph and image reconstruction parameters, thus minimizing the potential methodologic bias. Nonetheless, we acknowledge that scanning of mice on different days of the week, along with social hierarchy factors and technical factors due to different cage positions, might still impact the detection of plaque pathology by A β PET. We had to choose between conducting a longitudinal PET examination with immunochemistry/histochemistry in a separate cohort and conducting a cross-sectional study in which PET examination directly preceded immunohistochemistry/histochemistry in the same mice. Since animal-batch effects may introduce a bias into cross-sectional PET quantifications between different ages of a given mouse model, we elected to conduct longitudinal PET imaging together with cross-sectional immunochemistry and histochemistry to exclude batch effects, at least for PET. To account further for the heterogeneity (22) and asymmetry (13) of amyloidosis in individual mice of a lineage, we used a bilateral target in a regression model including each available combination of PET-immunochemistry/histochemistry results for each model at each of 3 ages, controlled for the individual heterogeneity. Regression coefficients for the proportions of fibrillar and nonfibrillar A β in different models were robust and revealed that fibrillar A β makes an intrinsically 16-fold higher contribution to the A β PET signal than nonfibrillar A β in the studied A β mouse models. Our preclinical in vivo results concur with the postmortem validation of human ¹⁸F-flutemetamol PET data, where

ligand binding to diffuse plaques was the most likely explanation for positive in vivo signals in patients who later proved to have only sparse neuritic plaques at autopsy (11,23). The same research group recently validated the contributions of diffuse and neuritic plaques to the ¹⁸F-flutemetamol and ¹¹C-Pittsburgh compound B autoradiography signals in an in vitro study (12). However, our study was the first translation of such findings into the in vivo setting and enables the arithmetic conversion of A β PET signals into fibrillar and nonfibrillar A β components. We note that the structure of the stilbene ¹⁸F-florbetaben is different from the structures of the benzothiazoles ¹⁸F-flutemetamol and ¹¹C-Pittsburgh compound B and that this difference could result in different proportions of fibrillar and nonfibrillar binding capacities in vivo. As usual, the limited resolution of small-animal PET systems in relation to the mouse brain size and resulting partial-volume effects present a limitation for the transfer of the present findings into the human context, and we want to emphasize that detailed regression factors cannot be transferred directly. Yet, the demonstration of an inherently 16-fold higher contribution of fibrillar plaque to the PET signal concurs with a biophysical chemistry study investigating binding mechanisms of A β ligands by molecular docking, molecular dynamics, and generalized Born-based free-energy calculations (24). Here, core sites of A β fibrils, which are more abundant in fibrillar components of the plaque, dominated over surface sites in producing the A β PET signal (24).

Our findings could be of translational relevance since A β -immunotherapy and other treatment strategies against AD may change the proportions of fibrillar and nonfibrillar plaque

components and thus bias the A β PET outcome. Furthermore, alterations of microglial genes are associated with changes in plaque morphology, which consequently influence the A β PET signal (5). We can correlate the more diffuse amyloid plaque morphology in *App^{NL-G-F}* mice with differences in plaque morphology observed in AD mice deficient in *TREM2* or *APOE* (5,25). Although loss-of-function mutations of *Trem2* are rare in humans, microglia genes seem in general (26) to have a high impact on AD pathology, and modulation of microglial function is being intensively studied as a therapeutic strategy for AD (27). Another limitation for the direct translation of our findings toward human AD consists in different binding site densities of A β plaques in A β mouse models when compared with sporadic AD (28). Thus, comparisons of A β PET signal intensity between rodents and humans need to be considered with caution. However, the regression model generated in this study should increase awareness of the impact of nonfibrillar A β on the A β PET signal in both species. Thus, a potential shift in the plaque proportions needs to be considered when designing future A β PET monitored studies that target microglia. Assessment of fibrillar and nonfibrillar plaque components and the respective A β PET tracer-binding properties in autopsy cases after or during disease-modifying treatment studies of AD could serve to test the impact of our findings on the human situation.

CONCLUSION

The A β PET signal with ¹⁸F-florbetaben in vivo arises from a combination of fibrillar and nonfibrillar plaque components. Fibrillar A β has inherently higher tracer binding, but the greater proportion of nonfibrillar A β relative to fibrillar A β in most plaques means that the nonfibrillar signal source is a relevant component of the total signal. Since experimental AD therapy regimens can shift the proportion of fibrillar versus nonfibrillar A β , any longitudinal changes in A β PET signal as a readout of therapy monitoring must be interpreted with caution; a detailed understanding of the biochemical basis of A β PET signal is critical for the correct use of PET for monitoring novel AD therapies.

DISCLOSURE

This work was supported by an Alzheimer's Association grant through the AD Strategic Fund (ADSF-21-831226-C) and by the German Research Foundation within the framework of the Munich Cluster for Systems Neurology (EXC 2145 SyNergy/ID 390857198). Sabina Tahirovic was supported by the Alzheimer-Forschung-Initiative e.V (grant 18014). Christian Haass collaborates with Denali Therapeutics, participated in one advisory board meeting of Biogen, and received a speaker honorarium from Novartis and Roche. Christian Haass is chief advisor of ISAR Bioscience. Peter Bartenstein, Axel Rominger, and Matthias Brendel received speaking honoraria from Life Molecular Imaging and GE Healthcare. Matthias Brendel is an advisor of Life Molecular Imaging. No other potential conflict of interest relevant to this article was reported.

ACKNOWLEDGMENTS

We thank Mathias Jucker for providing the APPPS1 mice and Takashi Saito and Takaomi C. Saido for providing the *App^{NL-G-F}* mice.

KEY POINTS

QUESTION: Does nonfibrillar A β contribute to the in vivo A β PET signal?

PERTINENT FINDINGS: Fibrillar A β has 16-fold higher tracer binding than does nonfibrillar A β , but the greater proportion of nonfibrillar A β relative to fibrillar A β in most plaques means that the nonfibrillar signal source is a relevant component of the total A β PET signal.

IMPLICATIONS FOR PATIENT CARE: Shifts of the proportion of fibrillar versus nonfibrillar A β need to be considered when interpreting the longitudinal A β PET signal for monitoring of therapeutic effects.

REFERENCES

- Koscik RL, Betthausen TJ, Jonaitis EM, et al. Amyloid duration is associated with preclinical cognitive decline and tau PET. *Alzheimers Dement (Amst)*. 2020;12:e12007.
- Jack CR Jr, Bennett DA, Blennow K, et al. NIA-AA research framework: toward a biological definition of Alzheimer's disease. *Alzheimers Dement*. 2018;14:535–562.
- Wessels AM, Tariot PN, Zimmer JA, et al. Efficacy and safety of lanabecestat for treatment of early and mild Alzheimer disease: the AMARANTH and DAYBREAK-ALZ randomized clinical trials. *JAMA Neurol*. 2020;77:199–209.
- Sevigny J, Chiao P, Bussière T, et al. The antibody aducanumab reduces A β plaques in Alzheimer's disease. *Nature*. 2016;537:50–56.
- Parhizkar S, Arzberger T, Brendel M, et al. Loss of TREM2 function increases amyloid seeding but reduces plaque-associated ApoE. *Nat Neurosci*. 2019;22:191–204.
- Overhoff F, Brendel M, Jaworska A, et al. Automated spatial brain normalization and hindbrain white matter reference tissue give improved [¹⁸F]-florbetaben PET quantitation in Alzheimer's model mice. *Front Neurosci*. 2016;10:45.
- Sabri O, Sabbagh MN, Seibyl J, et al. Florbetaben PET imaging to detect amyloid beta plaques in Alzheimer's disease: phase 3 study. *Alzheimers Dement*. 2015;11:964–974.
- Curtis C, Gamez JE, Singh U, et al. Phase 3 trial of flutemetamol labeled with radioactive fluorine 18 imaging and neuritic plaque density. *JAMA Neurol*. 2015;72:287–294.
- Rominger A, Brendel M, Burgold S, et al. Longitudinal assessment of cerebral b-amyloid deposition in mice overexpressing Swedish mutant b-amyloid precursor protein using ¹⁸F-florbetaben PET. *J Nucl Med*. 2013;54:1127–1134.
- Catafau AM, Bullich S, Seibyl JP, et al. Cerebellar amyloid-beta plaques: how frequent are they, and do they influence ¹⁸F-florbetaben SUV ratios? *J Nucl Med*. 2016;57:1740–1745.
- Ikonomic MD, Buckley CJ, Heurling K, et al. Post-mortem histopathology underlying beta-amyloid PET imaging following flutemetamol F 18 injection. *Acta Neuropathol Commun*. 2016;4:130.
- Ikonomic MD, Buckley CJ, Abrahamson EE, et al. Post-mortem analyses of PiB and flutemetamol in diffuse and cored amyloid-beta plaques in Alzheimer's disease. *Acta Neuropathol (Berl)*. 2020;140:463–476.
- Sacher C, Blume T, Beyer L, et al. Asymmetry of fibrillar plaque burden in amyloid mouse models. *J Nucl Med*. 2020;61:1825–1831.
- Sebastian Monasor L, Muller SA, Colombo AV, et al. Fibrillar Abeta triggers microglial proteome alterations and dysfunction in Alzheimer mouse models. *eLife*. 2020;9:e54083.
- Radde R, Bolmont T, Kaeser SA, et al. Abeta42-driven cerebral amyloidosis in transgenic mice reveals early and robust pathology. *EMBO Rep*. 2006;7:940–946.
- Masuda A, Kobayashi Y, Kogo N, Saito T, Saido TC, Itohara S. Cognitive deficits in single App knock-in mouse models. *Neurobiol Learn Mem*. 2016;135:73–82.
- Saito T, Matsuba Y, Mihira N, et al. Single App knock-in mouse models of Alzheimer's disease. *Nat Neurosci*. 2014;17:661–663.
- Sacher C, Blume T, Beyer L, et al. Longitudinal PET monitoring of amyloidosis and microglial activation in a second-generation amyloid-beta mouse model. *J Nucl Med*. 2019;60:1787–1793.

19. Yamasaki A, Eimer S, Okochi M, et al. The GxGD motif of presenilin contributes to catalytic function and substrate identification of gamma-secretase. *J Neurosci*. 2006;26:3821–3828.
20. Poisnel G, Dhilly M, Moustie O, et al. PET imaging with [¹⁸F]AV-45 in an APP/PS1-21 murine model of amyloid plaque deposition. *Neurobiol Aging*. 2012;33:2561–2571.
21. Mathis CA, Mason NS, Lopresti BJ, Klunk WE. Development of positron emission tomography beta-amyloid plaque imaging agents. *Semin Nucl Med*. 2012;42:423–432.
22. Brendel M, Jaworska A, Herms J, et al. Amyloid-PET predicts inhibition of de novo plaque formation upon chronic gamma-secretase modulator treatment. *Mol Psychiatry*. 2015;20:1179–1187.
23. Ikonomic MD, Fantoni ER, Farrar G, Salloway S. Infrequent false positive [¹⁸F]flutemetamol PET signal is resolved by combined histological assessment of neuritic and diffuse plaques. *Alzheimers Res Ther*. 2018;10:60.
24. Murugan NA, Halldin C, Nordberg A, Langstrom B, Agren H. The culprit is in the cave: the core sites explain the binding profiles of amyloid-specific tracers. *J Phys Chem Lett*. 2016;7:3313–3321.
25. Ulrich JD, Ulland TK, Mahan TE, et al. ApoE facilitates the microglial response to amyloid plaque pathology. *J Exp Med*. 2018;215:1047–1058.
26. Sierksma A, Lu A, Mancuso R, et al. Novel Alzheimer risk genes determine the microglia response to amyloid-beta but not to TAU pathology. *EMBO Mol Med*. 2020;12:e10606.
27. Lewcock JW, Schlepckow K, Di Paolo G, Tahirovic S, Monroe KM, Haass C. Emerging microglia biology defines novel therapeutic approaches for Alzheimer's disease. *Neuron*. 2020;108:801–821.
28. Klunk WE, Lopresti BJ, Ikonomic MD, et al. Binding of the positron emission tomography tracer Pittsburgh compound-B reflects the amount of amyloid-beta in Alzheimer's disease brain but not in transgenic mouse brain. *J Neurosci*. 2005;25:10598–10606.